Neural Progenitors as a Novel Pathogenic Mechanism in Microcephaly

Rami Yair Tshuva[1,2]†, Jeyoon Bok[3]†, Mio Nonaka[1,2], Xufeng Xue[3,4], Bidisha Bhattacharya[1,2], Aditya Kshirsagar[1], Tsviya Olender[1], Miri Danan-Gotthold[1], Tamar Sapir[1,2*], Jianping Fu[3,5,6*], and Orly Reiner[1,2*]

[1]Department of Molecular Genetics, Weizmann Institute of Science, Rehovot, Israel;

[2]Department of Molecular Neuroscience, Weizmann Institute of Science, Rehovot, Israel;

[3]Department of Mechanical Engineering, University of Michigan, Ann Arbor, MI, USA;

[4]Division of Developmental Biology, Center for Stem Cell and Organoid Medicine, Cincinnati Children's Hospital Medical Center, Cincinnati, OH, USA;

[5]Department of Biomedical Engineering, University of Michigan, Ann Arbor, MI, USA;

[6]Department of Cell & Developmental Biology, University of Michigan Medical School, Ann Arbor, MI, USA.

†These authors contributed equally to this work.

*Corresponding authors. Emails: orly.reiner@weizmann.ac.il, jpfu@umich.edu, tamar.sapir@weizmann.ac.il.

Abstract

Despite their significance, the genetic and molecular bases of neurodevelopmental disorders remain poorly understood. In this study, using human brain organoids and mouse models, we show that loss of *NDE1*, a gene closely associated with microcephaly, disrupts progenitor identity, prolongs mitosis, and alters regional patterning in the forebrain. *NDE1* knockout leads to a caudal identity shift of neural progenitor cells in the organoids and mouse brains, coinciding with aberrant ERK signaling. Notably, downstream activation of the ERK pathway restored rostral *PAX6* expression in human brain organoids. Parallel analyses of *Nde1* knockout mice confirmed disrupted regional patterning of the forebrain. Together, our data establish *NDE1* as a critical regulator of early human brain regionalization and elucidate molecular mechanisms underlying the structural abnormalities observed in *NDE1*-associated microcephaly.

Introduction

Neurodevelopmental disorders are among the most pressing challenges in modern medicine, yet their genetic and molecular bases remain poorly understood[1-4]. Recent stem cell-based models offer powerful experimental tools to dissect these disorders in human-relevant systems. Microcephaly is a particularly severe group of neurodevelopmental disorders marked by profound abnormalities in brain size and structure, including microlissencephaly, characterized by a small, smooth brain, and microhydranencephaly, in which most of the cerebral hemispheres are replaced by a liquid-filled, membranous structure[5-13]. One gene linked to microcephaly is *NDE1*, which encodes the NDE1 protein believed to act in concert with LIS1 to mediate cellular activities critical for brain development, including neuronal migration, mitotic spindle orientation, and RNA regulation[5-29]. Besides microcephaly, *NDE1* mutations have been associated with a range of other neurodevelopmental and psychiatric disorders, including schizophrenia, intellectual disabilities, and autism spectrum disorders[9-11,30-42]. Thus, understanding how *NDE1* mutations disrupt early brain development is critical to identifying the shared mechanisms that contribute to the wide range of complex phenotypes observed in neurodevelopmental disorders.

Results

To explore the roles of *NDE1*, we first examined its expression in the first-trimester human developing brain[43] (Fig. 1A-F). *NDE1* is expressed in cycling progenitors, and its expression peaks during the G2/M state, similar to Aurora-kinase (AURKA), a typical marker of this state. To examine the function of *NDE1*, we generated *NDE1* knockout (KO) human pluripotent stem cell (hPSC) lines (Fig. 1G), and the cell lines were differentiated into brain organoids using an unguided on-chip protocol[44] (Methods; Fig. 1H-L). The *NDE1* KO on-chip organoids displayed a reduced growth rate and decreased folding compared to wild-type (WT) controls (Fig. 1H-J). These findings are consistent with our previous work demonstrating that mutations in LIS1, a gene associated with lissencephaly, lead to diminished cortical folding[17,44]. Time-lapse imaging with H2B-mcherry and Lyn-GFP hPSCs enabled the analysis of specific phases of mitosis during brain organoid development (Fig. 1K-L). Overall, *NDE1* KO organoids exhibited a protracted duration of mitosis, with significant effects on prophase, metaphase, and telophase (Fig. 1L). Our findings fit the notion that many microcephaly-associated genes regulate the cell cycle[45-47].

We conducted bulk RNA-seq for the *NDE1* KO and WT hPSCs and the on-chip brain organoids derived from these cells on days 5 and 18 (Supplementary Data S1). Gene Analytics[48] analysis of differentially expressed genes (DEGs) revealed robust enrichment for "ERK Signaling" in the *NDE1* KO cells across developmental stages, peaking at the pluripotent stage and remaining elevated in brain organoids (Fig. 1M). Enrichment for "Nervous System Development" emerged at Day 5 and became more notable on Day 18, reflecting progressive neural differentiation and maturation (Fig. 1M). Further examination of DEGs revealed that in *NDE1* KO organoids, rostral genes, including *EMX2*, *LHX2*, and *PAX6*, were down-regulated, whereas caudal and ventral genes, including *EN2* and *DLX1*, were up-regulated, suggesting a shift in the regional identity of

neural progenitors in the organoids (Fig. 1N). These results were corroborated using real-time PCR (Supplementary Fig. S1A, Supplementary Table S1). Consistently, mouse models with reduced ERK signaling exhibit microcephaly[49,50], and furthermore, ERK signaling regulates PAX6 expression in the developing CNS[49].

Considering that the on-chip organoids are not patterned to a specific brain region identity, we sought additional strategies to examine the function of *NDE1* in brain patterning. To this end, we generated hPSC-derived organoids with either a cortical or cerebellar identity[51,52] (Methods; Supplementary Fig. S1B-H). *NDE1* KO cortical and cerebellar organoids both exhibited smaller sizes than WT controls (Supplementary Fig. S1B). However, the size disparity resulting from *NDE1* KO was more pronounced for cortical organoids. The smaller organoid size was not due to increased apoptosis, premature differentiation, or cell cycle exit (Supplementary Fig. S1C-H). Instead, phospho-histone immunostaining pointed toward differences in mitosis, consistent with previous studies[53] (Supplementary Fig. S1C-H).

We then conducted scRNA-seq for both *NDE1* KO and WT cortical organoids. A significant reduction in cells with a forebrain identity was noted in *NDE1* KO cortical organoids compared to WT controls (Fig. 2A, Supplementary Fig. S2A-G). When the regional identity of each cell was quantified, a significant decrease in the ratio of cells with forebrain, telencephalon, and diencephalon identities and an increase in the ratio of cells exhibiting the identities of midbrain, hindbrain, medulla, pons, and cerebellum were noted (Fig. 2B, Supplementary Fig. S2A-G). These regional fate identity changes were corroborated using real-time PCR, with *NDE1* KO cortical organoids exhibiting reduced expression of rostral genes, including *TBR1*, *EMX2*, and *FOXG1,* but upregulating caudal genes *EN1*, *EN2*, *PAX2*, and *IRX2* (Supplementary Fig. S2H). These convergent gene expression data support that *NDE1* loss disrupts early rostrocaudal brain patterning, diverting progenitors away from rostral forebrain fates and toward more caudal mid/hindbrain and cerebellar identities.

Current brain organoids usually do not recapitulate axial neural patterning within each individual structure. To address this limitation, we leveraged a recently developed NeuroMorphoChip (NMC)[54] system that applies microfluidic gradients for controlled formation of patterned neural organoids mimicking the entire CNS. By carefully adjusting microfluidic morphogen gradients, patterned forebrain-, midbrain-, and hindbrain-like regions could be induced in NMC organoids along their rostrocaudal axes (Methods; Fig. 2C,D). To investigate the role of *NDE1* in rostrocaudal neural patterning, immunostaining for PAX6 was conducted on both WT and *NDE1* KO NMC organoids. PAX6 is expressed in neuronal progenitors of the forebrain (covering telencephalon and diencephalon) and the hindbrain but is absent in the midbrain (Fig. 2E)[55]. In WT NMC tissues, PAX6 exhibited high expression in the rostral region corresponding to the forebrain, minimal expression in the mid-section associated with the midbrain, and moderate expression in the caudal, hindbrain-like area (Fig. 2F-I). In contrast, *NDE1* KO NMC organoids showed pronounced reduction in rostral PAX6 expression, accompanied by a notable expansion of caudal PAX6+ domains (Fig. 2F-I). This altered spatial patterning of PAX6 expression

underscores a critical role for *NDE1* in the proper regionalization of neural progenitors along the rostrocaudal axis.

scRNA-seq of the rostral halves of WT and *NDE1* KO NMC organoids further revealed a distinct cell cluster missing due to *NDE1* KO (Fig. 3A-C). This cluster is enriched for genes associated with signal transduction, cell cycle, mitosis, and ERK signaling (Fig. 3D, Supplementary Fig. S3A-L). When projected onto the data of radial glia from PCW 5 and 5.5 human brain atlas, the major progenitor population at this developmental stage, cells in the rostral halves of both WT and *NDE1* KO NMC tissues overlapped mainly with the forebrain radial glial cluster (Fig. 3E-G). Furthermore, the missing cell population in *NDE1* KO NMC organoids was also mainly projected to the forebrain region (Fig. 3H,I). Together, these data support that the rostral regions of *NDE1* KO NMC organoids were depleted of a subset of forebrain cells enriched with ERK signaling-related genes.

Our results point to dysregulated ERK signaling as a potential molecular mechanism underlying pathological brain patterning. To dissect ERK signaling in the context of *NDE1* deficiency, we first chose neural stem cells (NSCs) as a cellular model to investigate. Both *NDE1* KO and WT hPSCs were differentiated into NSCs, before these cells were stimulated with distinct ERK pathway activators, including EGF, FGF2, and phorbol 12-myristate 13-acetate (PMA) (Methods; Fig. 3J-O). Western blot analyses revealed that *NDE1* KO NSCs failed to mount a robust ERK phosphorylation response following EGF stimulation, in contrast to WT controls (Fig. 3J,K). Upon FGF2 treatment, ERK activation increased continuously in *NDE1* KO NSCs, as opposed to an attenuated activity in WT cells (Fig. 3L,M). Stimulation with PMA, a direct protein kinase C (PKC) activator that bypasses receptor-level inputs, restored ERK phosphorylation and nuclear translocation in *NDE1* KO NSCs to levels comparable to those observed for WT cells (Fig. 3N,O). Together, these data support that *NDE1* is required for upstream ERK pathway activation in response to specific morphogen signals. Nonetheless, *NDE1* KO might not impair the core signaling machinery downstream of MEK, including ERK activation and nuclear entry.

To corroborate the *in vitro* findings, we next generated *Nde1* KO mice and examined brain patterning (Methods; Fig. 4A-L), which was not reported in prior studies of *Nde1* KO mice[21]. Compared to WT controls, mutant mouse embryos exhibited a substantial decrease in PAX6 immunoreactivity in both the telencephalon and diencephalon (Fig. 4A-H,K). OTX2, typically upregulated in the forebrain and midbrain, was expressed in both WT and *Nde1* KO mouse brains (Fig. 4I-J,K). However, in WT mouse brains, OTX2 expression peaked in the diencephalon, while in *Nde1* KO ones it was maximal in the diencephalon (Fig. 4I,J,L). Thus, there is a notable caudal shift of the OTX2 expression peak to the midbrain due to *Nde1* KO.

Our on-chip brain organoids data revealed dysregulated ventral gene expression. We thus also examined two ventral markers in *Nde1* KO mouse brains: NKX2.2, which is primarily expressed in ventral forebrain, midbrain, and hindbrain, and NKX2.1, expressed in ventral forebrain, medial ganglionic eminence (MGE), and preoptic area (Fig. 4M-R)[56-58]. A striking difference was observed in NKX2.1 expression: while WT mouse brains displayed two distinct NKX2.1 expression domains, these areas appeared intermingled in mutant embryos (Fig. 4M-R).

Notably, in mouse brains, several regional identity markers - including FOXG1, PAX2, and PAX3 at the protein level, as well as *En1*, *Dlk1*, *Lmx1b*, and *Pax2* at the RNA level - remained largely unaffected by *Nde1* KO (Supplementary Fig. S3). These data suggest more subtle and specific patterning disruptions in mouse brains, as compared to the broader regional identity defects observed in the human models. Importantly, there was a decreased ERK activity, revealed by immunostaining for phosphorylated ERK, in *Nde1* KO mouse brains compared to WT controls (Fig. 4S-U).

We next examined whether ectopic activation of the ERK pathway could restore regional brain patterning in *NDE1* KO brain organoids. Given the importance of WNT inhibition in establishing forebrain identity[59], we included the WNT inhibitor XAV939 (XAV). XAV treatment alone of *NDE1* KO NMC organoids increased rostral expression of PAX6 similarly to PMA, and combining XAV with PMA resulted in an additive enhancement of PAX6 expression (Fig. 5A). Our experimental approach, detailed in Fig. 5B, therefore incorporated rostral addition of XAV. In *NDE1* KO NMC tissues, rostral *PAX6* RNA expression was significantly reduced (Fig. 5C). However, PMA treatment restored rostral *PAX6* RNA expression to control levels. All rescue or control groups (*NDE1* KO + PMA, WT, WT + PMA, all with XAV) displayed significantly greater rostral expression of PAX6, as compared to untreated *NDE1* KO NMC organoids. Spatial quantification further confirmed a pronounced increase in PAX6+ cells in PMA-treated *NDE1* KO NMC organoids (Fig. 5E). Together, these data show that downstream activation of the ERK pathway is sufficient to partially rescue impaired rostral PAX6 expression in *NDE1*-deficient brain organoids. The roles of NDE1 and LIS1 in the FGF-ERK pathway have been established in a previous limb development study, which supports the positioning of NDE1 and LIS1 both upstream and downstream of FGF receptor signaling[60].

In summary, this study unravels a previously unrecognized role of *NDE1* in regional patterning of neural progenitors in the brain. Using human brain organoids and mouse models, we show that loss of NDE1 impacts both brain size and regional identity (Fig. 5F). This patterning deficit was accompanied by dysregulated ERK signaling, which could be restored by downstream activation, rescuing PAX6 expression in *NDE1* KO brain organoids. Our data thus reveal a new mechanistic link between *NDE1*-mediated mitotic control and regional brain identity, mediated in part by ERK signaling associated with cytokines such as FGF and EGF. The rescue of rostral identity through ectopic activation of ERK signaling was also enhanced by WNT inhibition, suggesting cooperative interactions between these pathways in brain regional specification and demonstrating that dysregulation of brain regional patterning due to *NDE1* mutations might be partially reversible. Our data thus expand the classical view of NDE1 from being a “mitotic scaffold” that safeguards spindle orientation and progenitor pool size to a multifaceted regulator that also gates ERK signaling and, consequently, mediates brain regional patterning. Our data position NDE1 in the emerging category of microtubule-associated proteins as organizers of signaling complexes that coordinate proliferation dynamics with patterning signals, ensuring that daughter cells emerge with the correct regional identity rather than merely the correct number. The implications of this study are beyond just microcephaly, as ERK signaling might prove to be a viable therapeutic target in other neurodevelopmental disorders.

RNA-Seq data deposited

- MARSeq of on-chip organoids; To review GEO accession GSE232506: Go to https://www.ncbi.nlm.nih.gov/geo/query/acc.cgi?acc=GSE232506 Enter token cdqpqawmpbcjjav into the box
- scRNA-Seq of forebrain organoids; To review GEO accession GSE229988: Go to https://www.ncbi.nlm.nih.gov/geo/query/acc.cgi?acc=GSE229988 Enter token cdmfksoohjufben into the box
- scRNA-Seq of NeuroMorphoChip (NMC); To review GEO accession GSE279902: Go to https://www.ncbi.nlm.nih.gov/geo/query/acc.cgi?acc=GSE279902 Enter token sdgpamoanpwzryh into the box

Acknowledgments:

Orly Reiner is an incumbent of the Berstein-Mason professorial chair of Neurochemistry and the Head of the M. Judith Ruth Institute for Preclinical Brain Research. Tamar Sapir is the Incumbent of the Leir Research Fellow Chair in Autism Spectrum Disorder. We thank the transgenic mouse facility and the caretaker, Ms. Tamir Moshe, at the Weizmann Institute. Activities in the Fu lab have been supported technically by the Michigan Medicine Microscopy Core for microscopy imaging, the Michigan Advanced Genomics Core for scRNA-seq service, and the Michigan Lurie Nanofabrication Facility for microfabrication.

Funding:

Israel Science Foundation ISF grant (545/21)

United States-Israel Binational Science Foundation (BSF; Grant No. 2023009)

Israel Ministry of Innovation, Science and Technology IL (0005900)

Azrieli Institute for Brain and Neural Sciences

The Maurice and Vivienne Wohl Biology Endowment

The Gladys Monroy and Larry Marks Center for Brain Disorders

The Advantage Trust

The Nella and Leon Benoziyo Center for Neurological Diseases

The David and Fela Shapell Family Center for Genetic Disorders Research

The Abish-Frenkel RNA center

The Andrea L. and Lawrence A. Wolfe Family Center for Research on Neuroimmunology and Neuromodulation,

The Weizmann Center for Research on Neurodegeneration

The Brenden-Mann Women's Innovation Impact Fund

The Irving B. Harris Fund for New Directions in Brain Research

The Irving Bieber, M.D., and Toby Bieber, M.D. Memorial Research Fund

The Leff Family, Barbara & Roberto Kaminitz, Sergio & Sônia Lozinsky, Debbie Koren, Jack and Lenore Lowenthal, and the Dears Foundation

A research grant from the Estates of Ethel H. Smith, Gerald Alexander, Mr. and Mrs. George Zbeda, David A. Fishstrom, Norman Fidelman, Hermine Miller, Olga Klein Astrachan and Hermine Miller.

Ethel Lena Levy, the Selsky Memory Research Project

National Science Foundation of the United States (CBET 1901718, PFI 2213845, and EFMA 2422149)

National Institutes of Health of the United States (R21 NS127983, R01 GM143297, and R01 NS129850)

Author contributions:

Conceptualization: JF, TS, OR

Methodology: RYT, JB, MN, XX, AK

Investigation: RYT, JB, MN, AK, BB, TS, MDG

Visualization: RYT, JB, MN, BB, TS, MDG, TO

Funding acquisition: JF, OR

Project administration: JF, TS, OR

Supervision: XX, TO, MN, TS, JF, OR

Writing – original draft: OR, TS, JF

Writing – review & editing: RYT, JB, MN, XX, BB, AK, TO, MDG, TS, JF, OR

Competing interests:

Authors declare that they have no competing interests.

Data and materials availability: All data, code, and materials used in the analysis is available in some form to any researcher for purposes of reproducing or extending the analysis. Transfer of cell lines, mice, and plasmids will require materials transfer agreements (MTAs). RNA-seq accession numbers have been indicated.

Supplementary Materials

Materials and Methods

Figs. S1 to S4

Tables S1 to S2

References (*1-33*)

Data S1

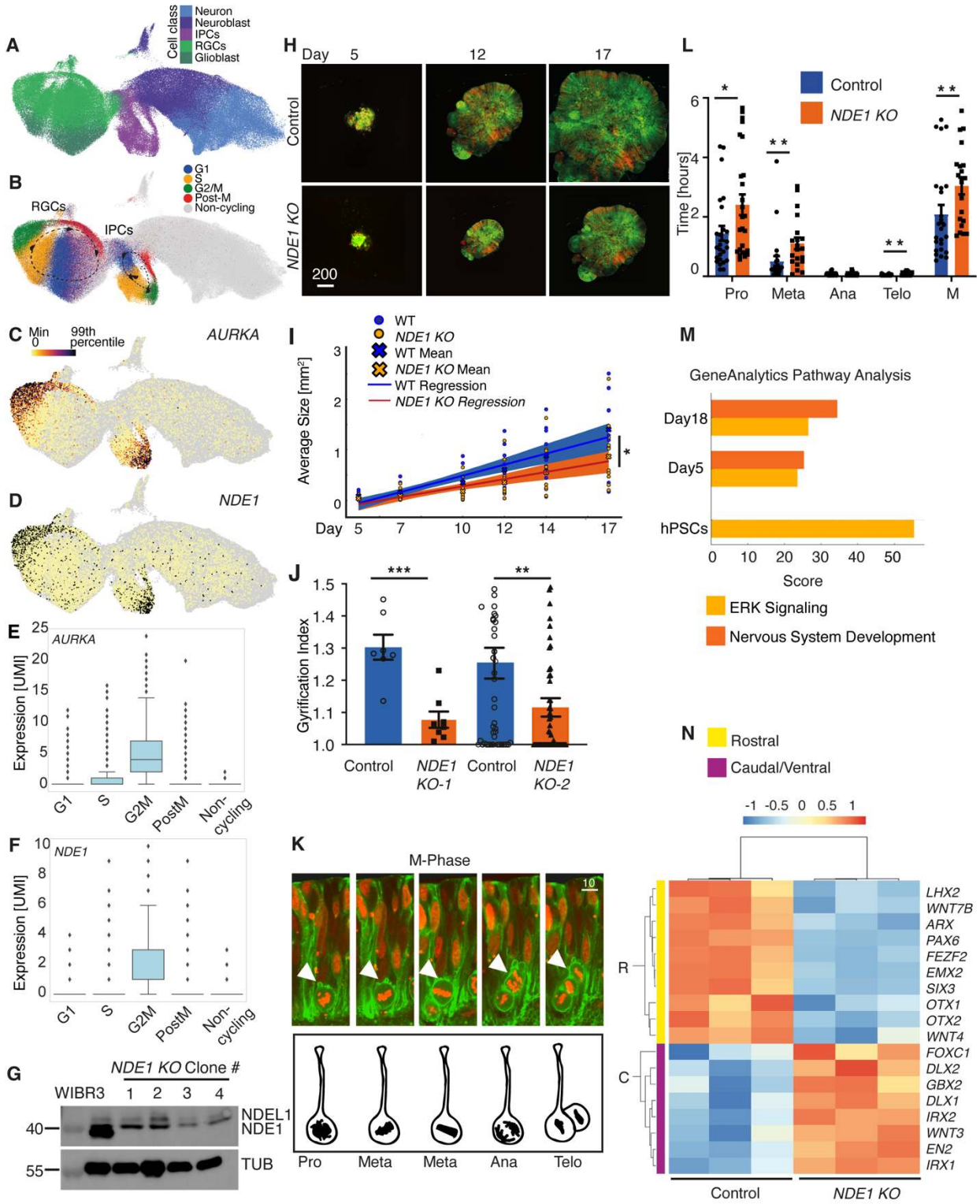

Fig. 1. Characterization of *NDE1* KO human on-chip brain organoids reveals disrupted progenitor identity and altered ERK signaling. (**A-D**) UMAP visualization of human cortical excitatory neuron lineage (EMX2-positive) (taken from Braun et al.[43]), colored by (**A**) major cell classes (RGCs, radial glia cells, IPCs, intermediate progenitor cells). (**B**) proliferation state (G1, S, G2M, post-M), non-cycling cells are colored in grey, (**C**) expression patterns of *AURKA* and (**D**) *NDE1,* note that both genes are highly expressed in cells at the G2/M state. (**E** and **F**) Box

plot of *AURKA* (**E**) and *NDE1* (**F**) expression across proliferation states (only v3 chemistry samples, see Methods). (**G**) Representative western blot showing the absence of NDE1 four *NDE1* KO clones used in this study. Tubulin serves as a loading control. (**H**) Representative images of WT and *NDE1* KO on-chip organoids at indicated differentiation days (5, 12, 17), labeled with H2B-mCherry (red) and Lyn-GFP (green). Scale bar, 200 µm. (**I**) Organoid size quantification (n ≥8 organoids per group, two biological repeats; the values were fitted on a linear growth curve showing the mean±SEM, the differences in the slopes are significant, P=0.0418*). (**J**) *NDE1* KO organoids exhibit fewer folds than the control, indicated by the gyrification index (mean ± SEM, WT n=7, *NDE1* KO-1 n=8, P=0.0006***, WT n=47, *NDE1* KO-2 n=55, P=0.042**, Mann–Whitney test). (**K**) Fluorescent time-lapse images of a dividing cell (indicated by the white arrowheads). The illustration below shows prophase (Pro), metaphase (Met), anaphase (Ana), and telophase (Tel). Scale bar, 10 µm. (**L**) Quantification of the mitosis (M) duration according to the indicated stages (mean ± SEM, WT n=20, *NDE1* KO n=25, Mann-Whitney test, prophase P=0.0276*, metaphase P=0.0013**, telophase P=0.0074**). (**M**) Histogram comparing GeneAnalytics scores for "ERK Signaling" Super Path and "Nervous System Development" pathways across developmental stages (hPSCs, Day 5, and Day 18). (**N**) Heatmap illustrating changes in regional marker gene expression across the rostrocaudal and dorsoventral axes in WT and *NDE1* KO organoids (color scale indicates normalized expression levels, n = 3).

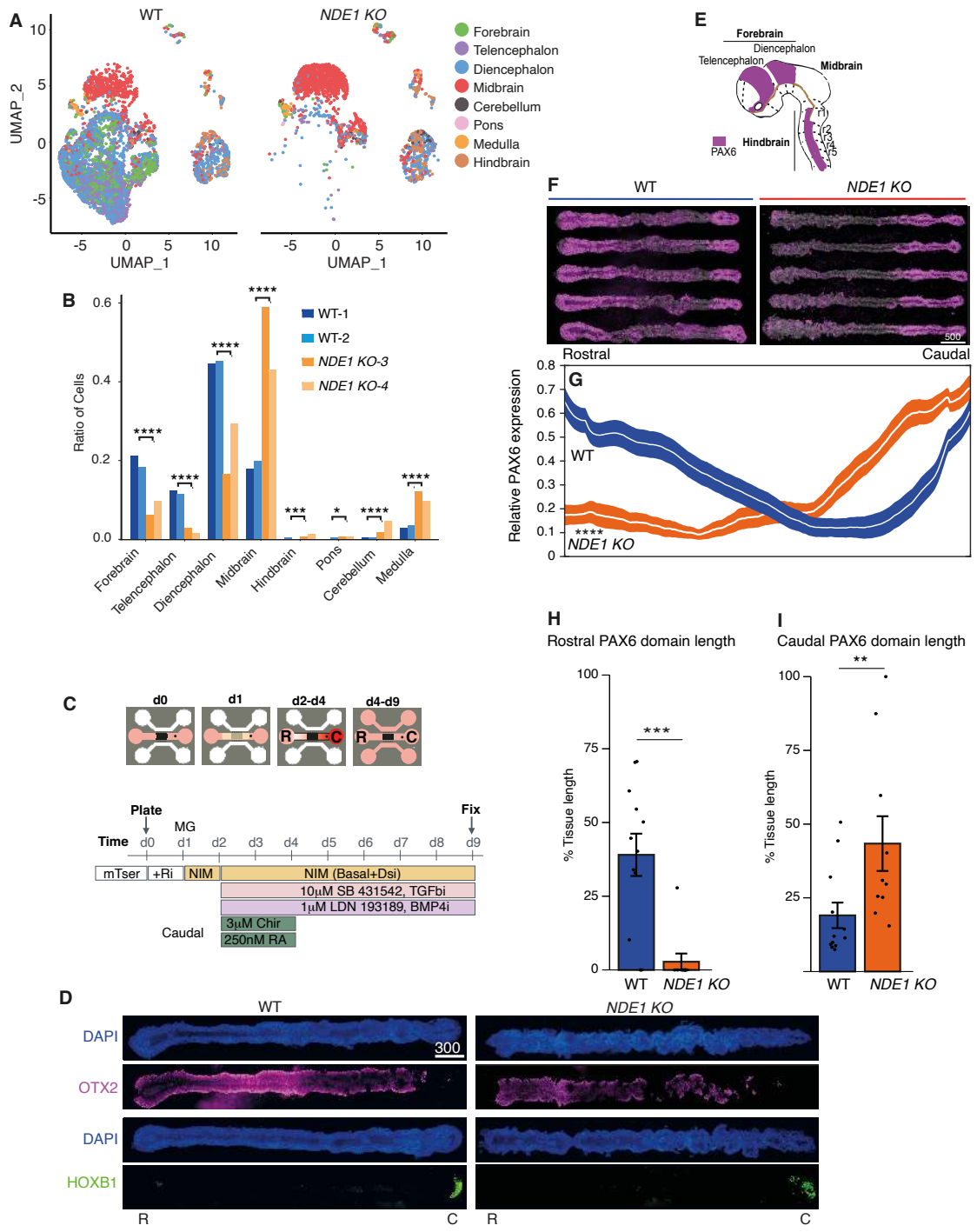

Fig. 2. Single-cell RNA analysis identifies altered progenitor identity and signaling. (A) UMAP of scRNA-Seq data of cortical organoids (Day 30). The regions are color-coded as indicated based on the human embryonic brain atlas[43]. (**B**) Barplot showing the ratio of WT and *NDE1* KO organoid cells mapped to each region (significance was determined by two-sided Fisher's exact test, *P<0.05, ***P<0.001, ****P<0.0001) (**C**) Schematic representation of rostrocaudal patterning strategy used for neural morpho chip (NMC) differentiation, including experimental timeline. (**D**) Representative immunofluorescence

images comparing regional marker protein expression (OTX2, HOXB1) combined with DAPI in WT and *NDE1* KO NMC. Rostral, R, and Caudal, C, sides are indicated (**scale bar: 300 µm**). (**E**) Schematic depicting PAX6 expression pattern in the rostral (forebrain, magenta) and caudal (hindbrain, magenta) domains. (**F**) Representative immunofluorescence images showing altered spatial distribution of PAX6-positive cells (magenta) in WT and *NDE1* KO NMCs (scale bar, 500 µm). (**G**) Quantification of the distribution of PAX6-positive cells along the rostrocaudal axis (mean ± SEM, n = 52 WT organoids and n = 36 KO organoids, functional ANOVA, permutation test). (**H**, **I**) Quantification of rostral (**H**) and caudal (**I**) PAX6 domain lengths in WT and *NDE1* KO NMCs, expressed as percentage of total organoid length (mean ± SEM, n = 13 WT NMCs and n = 10 KO NMCs; J, P =0.00032***, K, P=0.02894**, *Student's t-test*).

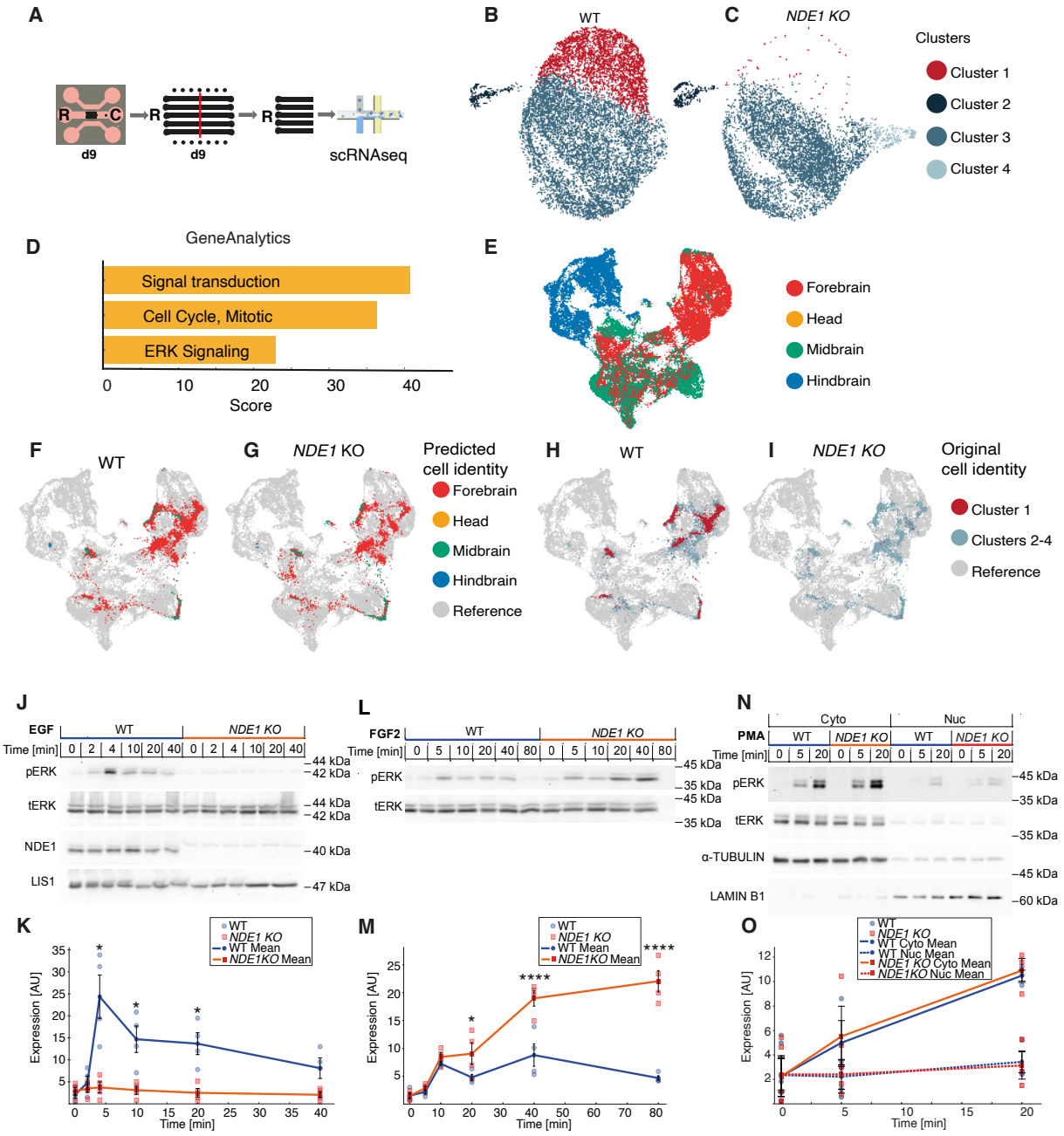

Fig. 3. scRNA-seq data and altered ERK signaling dynamics and regional identity in *NDE1* KO cells and NMCs. (**A**) Schematic representation of sample preparation for single-cell RNA sequencing. Tissues were cut in half, and the rostral halves were further processed. (**B**) UMAP revealed a missing cluster (cluster 1) in scRNA seq of the rostral halves of *NDE1* KO (**C**) compared to WT NMC's (**B**). (**D**) GeneAnalytics analysis of cluster 1 **(E-I)** UMAP visualization of 5 and 5.5 PCW radial glia cells from the human embryonic brain atlas[43], color-coded by anatomical region, (**F,G**) or the cluster identity **(H,I)** from **B** and **C**.

ERK signaling dynamics (**J-O**). (**J**, **L**, **N**) Representative western blots showing phosphorylated ERK (pERK) levels after stimulation with (**J**) EGF, (**L**) FGF2, and (**N**) PMA in WT and *NDE1* KO neural stem cells (NSCs). Total ERK (tERK) and β-actin were used as loading controls. (**K,M,O**) Quantification of western blot results from (**J**, **L**, **N**), respectively (mean ± SEM, n = 4 independent experiments, B, P<0.05*, D, P<0.00001****, F, all comparisons non-significant, Two Way ANOVA, posthoc Šídák's multiple comparisons test.

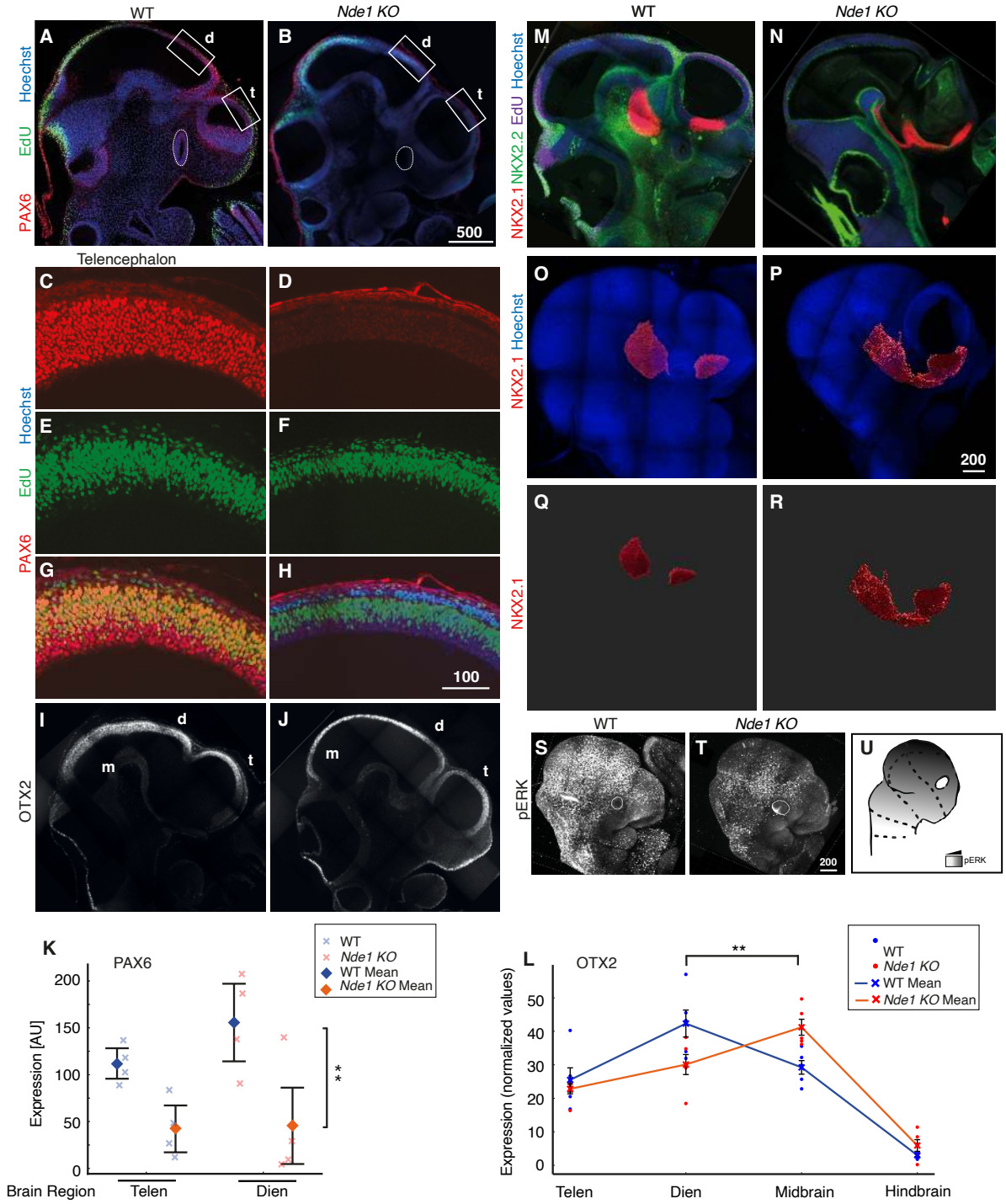

Fig. 4. Altered brain regionalization and signaling in *Nde1* KO mouse embryos.
(**A**, **B**) Immunofluorescence images of WT (**A**) and *Nde1* KO (**B**) Sagital optical Z slice from whole mount E10.5 mouse embryos stained for PAX6 (red), EdU (green), and Hoechst (blue); boxes indicate telencephalon (t) and diencephalon (d), the telencephalon regions are shown in

higher magnification below **(scale bar: 500 µm**). (**C-H**) High magnification of boxed t regions in (**A**, **B**) showing individual channels: PAX6 (red, **C, D**), EdU (green, **E, F**), and merged (**G, H**). Scale bar**: 100 µm.** (**I**, **J**) Immunofluorescence of OTX2 expression highlighting telencephalon (t), diencephalon (d), and midbrain (m) in WT (**I**) and KO (**J**) embryos (**scale bar: 200 µm**). (**K**, **L**) Quantification of PAX6 (**K**) and OTX2 (**L**) normalized expression intensity in WT and *Nde1* KO embryos. PAX6 data (**mean ± SEM; n = 4 embryos per genotype**) was analyzed using two-way ANOVA, genotype-based difference is significant P=0.0019**. OTX2 peak distribution (normalized values mean±SEM; WT, n=5, *Nde1* KO n=6) was analyzed by Fisher's exact test P=0.0022**. (**M-R**) Immunofluorescence images of NKX2.1 (red), **NKX2.2** (green), EdU (**magenta**), and Hoechst (blue) in WT (**M**) and KO (**N**) embryos illustrating ventral patterning changes (**scale bar: 200 µm**). (**O-R**) *Nde1-/-* NKX2.1 staining (red) shown alone as a volume using IMARIS and merged with Hoechst (blue), highlighting altered ventral domains in WT (**O, Q**) and KO (**P, R**) embryos. (**S-U**) Immunostaining for phosphorylated ERK (pERK) illustrating reduced ERK activation in *Nde1* KO (**T**) compared to WT (**S**) embryos; (**U**) shows a scheme of pERK expression pattern in the developing mouse embryonic brain.

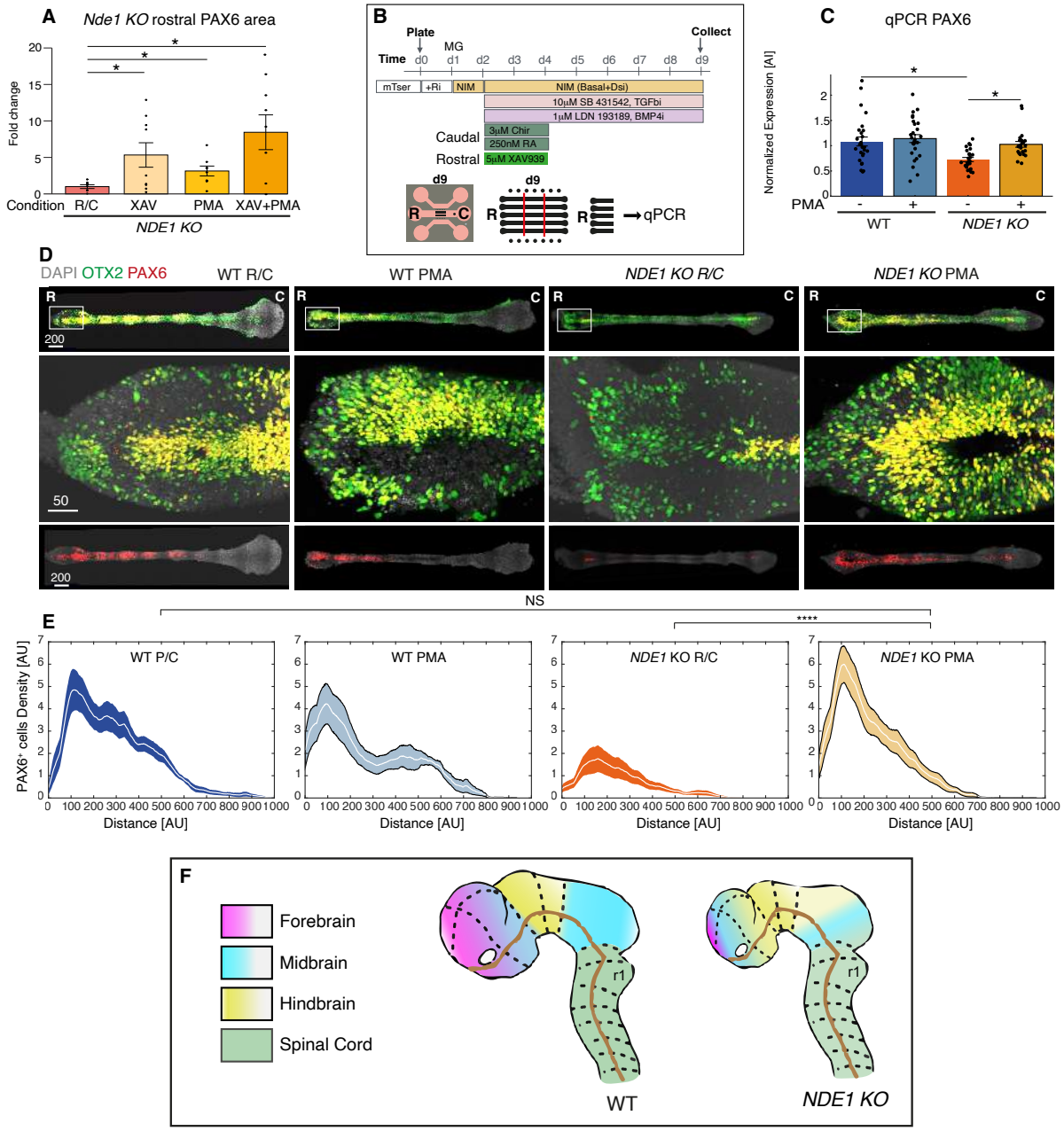

Fig. 5. ERK pathway activation restores rostral PAX6 expression in *NDE1* KO organoids. (**A**) Expansion of PAX6 rostral domain in NMC following addition of either the WNT inhibitor (XAV939, XAV), PMA, or both, to the rostral media reservoir during patterning. (**B**) Experimental timeline and schematic for PMA and WNT inhibitor (XAV939, XAV) treatments in NMC organoids. (**C**) qPCR quantification of normalized PAX6 rostral expression across wild-type (WT) and *NDE1* KO conditions, with and without PMA treatment. Each point represents a technical replicate; bars show mean ± SEM of biological replicates. Biological samples WT n=5, WT+PMA n=8, *NDE1* KO n=5, *NDE1* KO+ PMA n=4. A linear mixed-effects model was

applied with Genotype and Treatment as fixed effects and Biological Replicate as a random intercept. Significant differences were observed between WT and *NDE1* KO($p < 0.05$), and between *NDE1* KO and *NDE1* KO+PMA ($p < 0.05$), indicating that PMA partially rescues PAX6 expression in NDE1 organoids. No significant interaction was found between Genotype and Treatment. (**D**) Representative immunofluorescence images showing expression of PAX6 (red), OTX2 (green), and DAPI (gray) in *NDE1* KO organoids with and without PMA treatment; magnified regions indicated by boxes (scale bars: 200µm for the top and bottom images and 50µm for the middle panel). (**E**) Quantification of spatial distribution of PAX6-positive cells along the rostrocaudal axis in WT control (dark blue), WT+PMA (light blue), NDE1 KO (orange), and NDE1 KO+PMA (light orange) organoids. Shaded areas represent SEM; (WT n=9, WT + PMA n=7, *NDE1* KO n=9, *NDE1* KO + PMA n=10 fANOVA, permutation test was used for statistical test, significance P=0****, or NS, non-significant). (**F**) Schematic summarizing the regional identity shifts observed with *NDE1* KO in comparison to WT organoids (colors represent regions: pink = rostral forebrain; yellow = midbrain; blue = hindbrain; green = spinal cord).

References

1 Parrini, E., Conti, V., Dobyns, W. B. & Guerrini, R. Genetic Basis of Brain Malformations. *Mol Syndromol* **7**, 220-233 (2016). https://doi.org/10.1159/000448639

2 Oegema, R. *et al.* International consensus recommendations on the diagnostic work-up for malformations of cortical development. *Nat Rev Neurol* **16**, 618-635 (2020). https://doi.org/10.1038/s41582-020-0395-6

3 Ross, M. E. & Walsh, C. A. Human brain malformations and their lessons for neuronal migration. *Annu Rev Neurosci* **24**, 1041-1070 (2001). https://doi.org/10.1146/annurev.neuro.24.1.1041

4 Di Lullo, E. & Kriegstein, A. R. The use of brain organoids to investigate neural development and disease. *Nat Rev Neurosci* **18**, 573-584 (2017). https://doi.org/10.1038/nrn.2017.107

5 Alkuraya, F. S. *et al.* Human mutations in NDE1 cause extreme microcephaly with lissencephaly [corrected]. *American journal of human genetics* **88**, 536-547 (2011). https://doi.org/10.1016/j.ajhg.2011.04.003

6 Bakircioglu, M. *et al.* The essential role of centrosomal NDE1 in human cerebral cortex neurogenesis. *American journal of human genetics* **88**, 523-535 (2011). https://doi.org/10.1016/j.ajhg.2011.03.019

7 Ghannad, M. The essential role of NDE1 in extreme microcephaly. *Clin Genet* **80**, 241-242 (2011). https://doi.org/10.1111/j.1399-0004.2011.01753.x

8 Guven, A., Gunduz, A., Bozoglu, T. M., Yalcinkaya, C. & Tolun, A. Novel NDE1 homozygous mutation resulting in microhydranencephaly and not microlyssencephaly. *Neurogenetics* **13**, 189-194 (2012). https://doi.org/10.1007/s10048-012-0326-9

9 Paciorkowski, A. R. *et al.* Deletion 16p13.11 uncovers NDE1 mutations on the non-deleted homolog and extends the spectrum of severe microcephaly to include fetal brain disruption. *Am J Med Genet A* **161A**, 1523-1530 (2013). https://doi.org/10.1002/ajmg.a.35969

10 Sajan, S. A. *et al.* Both rare and de novo copy number variants are prevalent in agenesis of the corpus callosum but not in cerebellar hypoplasia or polymicrogyria. *PLoS Genet* **9**, e1003823 (2013). https://doi.org/10.1371/journal.pgen.1003823

11 Tan, L. *et al.* Severe congenital microcephaly with 16p13.11 microdeletion combined with NDE1 mutation, a case report and literature review. *BMC Med Genet* **18**, 141 (2017). https://doi.org/10.1186/s12881-017-0501-9

12 Abdel-Hamid, M. S., El-Dessouky, S. H., Ateya, M. I., Gaafar, H. M. & Abdel-Salam, G. M. H. Phenotypic spectrum of NDE1-related disorders: from microlissencephaly to microhydranencephaly. *Am J Med Genet A* **179**, 494-497 (2019). https://doi.org/10.1002/ajmg.a.61035

13 Bas, H. *et al.* NDE1-related disorders: A recurrent NDE1 pathogenic variant causing Lissencephaly 4 can also be associated with microhydranencephaly. *Am J Med Genet A* **188**, 326-331 (2022). https://doi.org/10.1002/ajmg.a.62508

14 Kshirsagar, A. & Reiner, O. in *Neocortical Neurogenesis in Development and Evolution* 365-396 (2023).

15 Efimov, V. P. & Morris, N. R. The LIS1-related NUDF protein of Aspergillus nidulans interacts with the coiled-coil domain of the NUDE/RO11 protein. *J Cell Biol* **150**, 681-688 (2000). https://doi.org/10.1083/jcb.150.3.681

16 Hoffmann, B., Zuo, W., Liu, A. & Morris, N. R. The LIS1-related protein NUDF of Aspergillus nidulans and its interaction partner NUDE bind directly to specific subunits

of dynein and dynactin and to alpha- and gamma-tubulin. *J Biol Chem* **276**, 38877-38884 (2001). https://doi.org/10.1074/jbc.M106610200

17 Reiner, O. *et al.* Isolation of a Miller-Dieker lissencephaly gene containing G protein beta-subunit-like repeats. *Nature* **364**, 717-721 (1993). https://doi.org/10.1038/364717a0

18 Hoffmann, B., Zuo, W., Liu, A. & Morris, N. R. The LIS1-related protein NUDF of Aspergillus nidulans and its interaction partner NUDE bind directly to specific subunits of dynein and dynactin and to alpha- and gamma-tubulin. *J Biol Chem* **279**, 820 (2004).

19 Stehman, S. A., Chen, Y., McKenney, R. J. & Vallee, R. B. NudE and NudEL are required for mitotic progression and are involved in dynein recruitment to kinetochores. *J Cell Biol* **178**, 583-594 (2007). https://doi.org/10.1083/jcb.200610112

20 Niethammer, M. *et al.* NUDEL is a novel Cdk5 substrate that associates with LIS1 and cytoplasmic dynein. *Neuron* **28**, 697-711 (2000). https://doi.org/10.1016/s0896-6273(00)00147-1

21 Feng, Y. & Walsh, C. A. Mitotic spindle regulation by Nde1 controls cerebral cortical size. *Neuron* **44**, 279-293 (2004). https://doi.org/10.1016/j.neuron.2004.09.023

22 Efimov, V. P. Roles of NUDE and NUDF proteins of Aspergillus nidulans: insights from intracellular localization and overexpression effects. *Mol Biol Cell* **14**, 871-888 (2003). https://doi.org/10.1091/mbc.e02-06-0359

23 Efimov, V. P., Zhang, J. & Xiang, X. CLIP-170 homologue and NUDE play overlapping roles in NUDF localization in Aspergillus nidulans. *Mol Biol Cell* **17**, 2021-2034 (2006). https://doi.org/10.1091/mbc.e05-11-1084

24 Feng, Y. *et al.* LIS1 regulates CNS lamination by interacting with mNudE, a central component of the centrosome. *Neuron* **28**, 665-679 (2000). https://doi.org/10.1016/s0896-6273(00)00145-8

25 Fridolfsson, H. N., Ly, N., Meyerzon, M. & Starr, D. A. UNC-83 coordinates kinesin-1 and dynein activities at the nuclear envelope during nuclear migration. *Dev Biol* **338**, 237-250 (2010). https://doi.org/10.1016/j.ydbio.2009.12.004

26 Kitagawa, M. *et al.* Direct association of LIS1, the lissencephaly gene product, with a mammalian homologue of a fungal nuclear distribution protein, rNUDE. *Febs Lett* **479**, 57-62 (2000). https://doi.org/10.1016/s0014-5793(00)01856-1

27 McKenney, R. J., Vershinin, M., Kunwar, A., Vallee, R. B. & Gross, S. P. LIS1 and NudE induce a persistent dynein force-producing state. *Cell* **141**, 304-314 (2010). https://doi.org/10.1016/j.cell.2010.02.035

28 Tarricone, C. *et al.* Coupling PAF signaling to dynein regulation: structure of LIS1 in complex with PAF-acetylhydrolase. *Neuron* **44**, 809-821 (2004). https://doi.org/10.1016/j.neuron.2004.11.019

29 Yan, X. *et al.* Human Nudel and NudE as regulators of cytoplasmic dynein in poleward protein transport along the mitotic spindle. *Mol Cell Biol* **23**, 1239-1250 (2003). https://doi.org/10.1128/MCB.23.4.1239-1250.2003

30 Balasubramanian, M., Smith, K., Mordekar, S. R. & Parker, M. J. Clinical report: AN INTERSTITIAL deletion of 16p13.11 detected by array CGH in a patient with infantile spasms. *Eur J Med Genet* **54**, 314-318 (2011). https://doi.org/10.1016/j.ejmg.2011.01.008

31 Ramalingam, A. *et al.* 16p13.11 duplication is a risk factor for a wide spectrum of neuropsychiatric disorders. *J Hum Genet* **56**, 541-544 (2011). https://doi.org/10.1038/jhg.2011.42

32 Liu, J. Y., Kasperaviciute, D., Martinian, L., Thom, M. & Sisodiya, S. M. Neuropathology of 16p13.11 deletion in epilepsy. *PLoS One* **7**, e34813 (2012). https://doi.org/10.1371/journal.pone.0034813

33 Tropeano, M. *et al.* Male-biased autosomal effect of 16p13.11 copy number variation in neurodevelopmental disorders. *PLoS One* **8**, e61365 (2013). https://doi.org/10.1371/journal.pone.0061365

34 Johnstone, M. *et al.* Copy Number Variations in DISC1 and DISC1-Interacting Partners in Major Mental Illness. *Mol Neuropsychiatry* **1**, 175-190 (2015). https://doi.org/10.1159/000438788

35 Kimura, H. *et al.* Identification of Rare, Single-Nucleotide Mutations in NDE1 and Their Contributions to Schizophrenia Susceptibility. *Schizophr Bull* **41**, 744-753 (2015). https://doi.org/10.1093/schbul/sbu147

36 Bradshaw, N. J. Cloning of the promoter of NDE1, a gene implicated in psychiatric and neurodevelopmental disorders through copy number variation. *Neuroscience* **324**, 262-270 (2016). https://doi.org/10.1016/j.neuroscience.2016.03.018

37 Brownstein, C. A. *et al.* Overlapping 16p13.11 deletion and gain of copies variations associated with childhood onset psychosis include genes with mechanistic implications for autism associated pathways: Two case reports. *Am J Med Genet A* **170A**, 1165-1173 (2016). https://doi.org/10.1002/ajmg.a.37595

38 Johnstone, M. *et al.* Reversal of proliferation deficits caused by chromosome 16p13.11 microduplication through targeting NFkappaB signaling: an integrated study of patient-derived neuronal precursor cells, cerebral organoids and in vivo brain imaging. *Mol Psychiatry* **24**, 294-311 (2019). https://doi.org/10.1038/s41380-018-0292-1

39 Allach El Khattabi, L. *et al.* 16p13.11 microduplication in 45 new patients: refined clinical significance and genotype-phenotype correlations. *J Med Genet* **57**, 301-307 (2020). https://doi.org/10.1136/jmedgenet-2018-105389

40 Buttermore, E. D. *et al.* 16p13.11 deletion variants associated with neuropsychiatric disorders cause morphological and synaptic changes in induced pluripotent stem cell-derived neurons. *Front Psychiatry* **13**, 924956 (2022). https://doi.org/10.3389/fpsyt.2022.924956

41 Okumura, H., Arioka, Y., Kushima, I., Mori, D. & Ozaki, N. Establishment of induced pluripotent stem cells from a patient with 16p13.11 duplication and VPS13B deletion. *Stem Cell Res* **64**, 102884 (2022). https://doi.org/10.1016/j.scr.2022.102884

42 Kimura, H. *et al.* Clinical characterization of patients with schizophrenia and 16p13.11 duplication: A case series. *Neuropsychopharmacol Rep* **43**, 267-271 (2023). https://doi.org/10.1002/npr2.12334

43 Braun, E. *et al.* Comprehensive cell atlas of the first-trimester developing human brain. *Science* **382**, eadf1226 (2023). https://doi.org/10.1126/science.adf1226

44 Karzbrun, E., Kshirsagar, A., Cohen, S. R., Hanna, J. H. & Reiner, O. Human Brain Organoids on a Chip Reveal the Physics of Folding. *Nat Phys* **14**, 515-522 (2018). https://doi.org/10.1038/s41567-018-0046-7

45 Faheem, M. *et al.* Molecular genetics of human primary microcephaly: an overview. *BMC Med Genomics* **8 Suppl 1**, S4 (2015). https://doi.org/10.1186/1755-8794-8-S1-S4

46 Gabriel, E., Ramani, A., Altinisik, N. & Gopalakrishnan, J. Human Brain Organoids to Decode Mechanisms of Microcephaly. *Front Cell Neurosci* **14**, 115 (2020). https://doi.org/10.3389/fncel.2020.00115

47 Gilmore, E. C. & Walsh, C. A. Genetic causes of microcephaly and lessons for neuronal development. *Wiley Interdiscip Rev Dev Biol* **2**, 461-478 (2013). https://doi.org/10.1002/wdev.89

48 Ben-Ari Fuchs, S. *et al.* GeneAnalytics: An Integrative Gene Set Analysis Tool for Next Generation Sequencing, RNAseq and Microarray Data. *OMICS* **20**, 139-151 (2016). https://doi.org/10.1089/omi.2015.0168

49 Pucilowska, J., Puzerey, P. A., Karlo, J. C., Galan, R. F. & Landreth, G. E. Disrupted ERK signaling during cortical development leads to abnormal progenitor proliferation, neuronal and network excitability and behavior, modeling human neuro-cardio-facial-cutaneous and related syndromes. *J Neurosci* **32**, 8663-8677 (2012). https://doi.org/10.1523/JNEUROSCI.1107-12.2012

50 Pucilowska, J. *et al.* The 16p11.2 deletion mouse model of autism exhibits altered cortical progenitor proliferation and brain cytoarchitecture linked to the ERK MAPK pathway. *J Neurosci* **35**, 3190-3200 (2015). https://doi.org/10.1523/JNEUROSCI.4864-13.2015

51 Sakaguchi, H. *et al.* Generation of functional hippocampal neurons from self-organizing human embryonic stem cell-derived dorsomedial telencephalic tissue. *Nature communications* **6**, 1-11 (2015).

52 Watanabe, M. *et al.* Self-Organized Cerebral Organoids with Human-Specific Features Predict Effective Drugs to Combat Zika Virus Infection. *Cell Rep* **21**, 517-532 (2017). https://doi.org/10.1016/j.celrep.2017.09.047

53 Suresh, V. *et al.* PRDM16 co-operates with LHX2 to shape the human brain. *Oxf Open Neurosci* **3**, kvae001 (2024). https://doi.org/10.1093/oons/kvae001

54 Xue, X. *et al.* A patterned human neural tube model using microfluidic gradients. *Nature* **628**, 391-399 (2024). https://doi.org/10.1038/s41586-024-07204-7

55 Stoykova, A. & Gruss, P. Roles of Pax-genes in developing and adult brain as suggested by expression patterns. *J Neurosci* **14**, 1395-1412 (1994). https://doi.org/10.1523/JNEUROSCI.14-03-01395.1994

56 Sussel, L., Marin, O., Kimura, S. & Rubenstein, J. L. Loss of Nkx2.1 homeobox gene function results in a ventral to dorsal molecular respecification within the basal telencephalon: evidence for a transformation of the pallidum into the striatum. *Development* **126**, 3359-3370 (1999). https://doi.org/10.1242/dev.126.15.3359

57 Briscoe, J. *et al.* Homeobox gene Nkx2.2 and specification of neuronal identity by graded Sonic hedgehog signalling. *Nature* **398**, 622-627 (1999). https://doi.org/10.1038/19315

58 Puelles, L. *et al.* Pallial and subpallial derivatives in the embryonic chick and mouse telencephalon, traced by the expression of the genes Dlx-2, Emx-1, Nkx-2.1, Pax-6, and Tbr-1. *J Comp Neurol* **424**, 409-438 (2000). https://doi.org/10.1002/1096-9861(20000828)424:3<409::aid-cne3>3.0.co;2-7

59 Watanabe, K. *et al.* Directed differentiation of telencephalic precursors from embryonic stem cells. *Nat Neurosci* **8**, 288-296 (2005). https://doi.org/10.1038/nn1402

60 Liu, L. *et al.* The LIS1/NDE1 Complex Is Essential for FGF Signaling by Regulating FGF Receptor Intracellular Trafficking. *Cell Rep* **22**, 3277-3291 (2018). https://doi.org/10.1016/j.celrep.2018.02.077